Iron-Induced Acceptor Centers in the Gallium Nitride High Electron Mobility Transistor: Thermal Simulation and Analysis

Vladislav Volcheck, Viktor Stempitsky
Department of Radioengineering and Electronics
Belarusian State University of Informatics and Radioelectronics
6 Petrusya Brovki St Minsk 220013 Belarus
vlad.volchek@bsuir.by

Dao Dinh Ha, Tran Tuan Trung, Nguyen Trong Quang
Le Quy Don Technical University
Hanoi, Vietnam
havixuly@gmail.com

***Abstract*—The effect of the presence of iron-induced acceptor centers in the gallium nitride high electron mobility transistor is studied using device physics simulations at elevated temperatures, as a lattice heat flow equation is solved self-consistently with the Poisson and the continuity equations to account for self-heating effects. It is shown that the acceptor centers intentionally introduced in the buffer layer of the device cause a shift of the input characteristics in the positive direction.**

I. Introduction

Gallium nitride (GaN) is a binary III/V semiconductor with a wide band gap of 3.4 eV, which affords it outstanding properties for applications in high power, high frequency and optoelectronic devices. The excellent breakdown and reasonable transport characteristics of GaN are made full use of in heterojunction field-effect transistors or high electron mobility transistors (HEMTs), which are currently the most widespread electronic nitride devices. The HEMT is a field-effect transistor, incorporating a junction between two materials with different band gaps, i.e. heterojunction, to confine electrons to a triangular quantum well.

Unlike the case of some other popular III/V materials such as gallium arsenide and indium phosphide, GaN substrates have only recently been commercially available in semi-insulating and n-conducting forms with diameters suitable for electronic device fabrication [1]. The high-pressure growth, processing and dc characterization of HEMTs over semi-insulating bulk GaN substrates were first reported by Khan et al. in 2000 [2]. A continuous-wave power density of 9.4 W/mm at 10 GHz with an associated power-added efficiency of 40 % was obtained by Chu et al. in 2004 for HEMTs on low-dislocation semi-insulting GaN substrates [3]. However, the size and quality limitations and the high production cost of free-standing GaN wafers have yet to be overcome for the commercial success of the GaN-on-GaN technology.

For modern power electronics and microwave applications, GaN films are generally grown at a high temperature by metal organic chemical vapor deposition (MOCVD) or molecular beam epitaxy techniques on silicon, sapphire or silicon carbide substrates. Nowadays, the fabrication of GaN HEMTs is conducted mainly by MOCVD due to its high efficiency and adequate precision. A major problem for nonoptimized growth conditions is unintentional doping responsible for a very high background donor concentration and thus persistent electron conductivity. The n-type conductivity of GaN films had earlier been ascribed to the formation of nitrogen vacancies in the GaN crystal [4]. According to a more detailed research, though, the major source of residual electrons is oxygen, an omnipresent shallow-level donor impurity in the MOCVD reactor [5]. Since the buffer layer in the HEMT structure must be designed to insulate the device and confine electrons in the channel, the residual donors should be compensated by deep-level acceptor centers to obtain high resistivity. In [6], the use of iron (Fe) doping to suppress the premature off-state breakdown in GaN HEMTs is described. In this paper, we investigate the effect of the presence of Fe-induced deep-level acceptor centers treated as trap states on the dc characteristics of the GaN HEMT using device physics simulations at elevated temperatures.

II. Structure

A two-dimensional schematic representation of the GaN HEMT device structure is shown in Fig. 1. The heterostructure consists of a 1.5 μm GaN buffer layer and a 20 nm aluminum gallium nitride ($Al_{0.21}Ga_{0.79}N$) barrier layer. The thickness and the length of the gate are equal to 3 μm and 0.5 μm, respectively.

XXX-X-XXXX-XXXX-X/XX/$XX.00 ©20XX IEEE

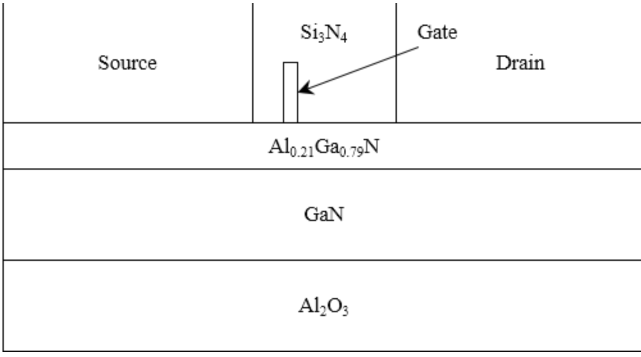

Fig. 1. GaN HEMT structure

The source-to-gate and the gate-to-drain distances are 1 μm and 3.5 μm, respectively.

The surface of the structure is passivated by a 6 μm silicon nitride (Si_3N_4) layer. The thickness of the sapphire (Al_2O_3) substrate is 1 μm. The length of the whole structure is 8 μm and the scale factor representing the third dimension (unsimulated) in two-dimensional simulations is 150 μm.

III. Simulation Details

The electrical behavior of a semiconductor device is operated by a mathematical model, which consists of a coupled set of basic partial differential equations linking together the electrostatic potential and the carrier concentration. The general framework of the model is provided by the Poisson and carrier continuity equations. To account for self-heating effects, a lattice heat flow equation is solved self-consistently with the primary equations.

A. Poisson and Carrier Continuity Equations

The Poisson equation governs the interaction of the electrostatic potential with the space charge density:

$$\nabla^2\varphi = \frac{q\left(N_d - N_a - n + p\right)}{\varepsilon\varepsilon_0}, \quad (1)$$

where φ is the electrostatic potential, q is the elementary charge, N_d and N_a are the donor and acceptor densities, n and p are the electron and hole concentrations, ε is the relative permittivity and ε_0 is the electric constant.

The continuity equations describe the way the electron and hole concentrations evolve as a result of the transport, generation and recombination processes. In a steady state, the generation and recombination rates are equal, the electron and hole concentrations are constant and the continuity equations are given as follows:

$$q\frac{\partial n}{\partial t} = \nabla J_n = 0, \quad (2)$$

$$q\frac{\partial p}{\partial t} = \nabla J_p = 0, \quad (3)$$

where J_n and J_p are the electron and hole current densities (for simplicity, referred to hereafter as the currents).

In accordance with the drift-diffusion transport theory, the driving force for the carriers is the quasi-Fermi level gradients:

$$J_n = q\mu_n n\nabla\varphi_n, \quad (4)$$

$$J_p = q\mu_p p\nabla\varphi_p, \quad (5)$$

where μ_n and μ_p are the electron and hole mobilities, φ_n and φ_p are the quasi-Fermi levels for electrons and holes.

By neglecting the gradient of the intrinsic carrier concentration, the currents can be decomposed into the drift and diffusion ingredients:

$$J_n = q\mu_n nE + qD_n\nabla n, \quad (6)$$

$$J_p = q\mu_p pE + qD_p\nabla p, \quad (7)$$

where D_n and D_p are the diffusivities and E denotes the electric field related to the potential through the Gauss law:

$$E = -\nabla\varphi. \quad (8)$$

It should be noted that the Einstein relationship is tacitly assumed to hold:

$$D_n = V_T\mu_n, \quad (9)$$

$$D_p = V_T\mu_p, \quad (10)$$

where V_T is the thermal voltage:

$$V_T = \frac{\kappa T}{q}, \quad (11)$$

where κ is the Boltzmann constant and T is the temperature.

In case of a single AlGaN/GaN heterostructure, GaN is specified as a reference material, since it has a lower band gap. The electron and hole concentrations are linked to the potential in AlGaN through the following expressions:

$$n = \frac{n_i^{\mathrm{GaN}} N_c^{\mathrm{AlGaN}}}{N_c^{\mathrm{GaN}}}\exp\left(\frac{\varphi + \varphi_n - \chi^{\mathrm{GaN}} + \chi^{\mathrm{AlGaN}}}{V_T}\right), \quad (12)$$

$$p = \frac{\left(n_i^{\mathrm{AlGaN}}\right)^2 N_c^{\mathrm{GaN}}}{n_i^{\mathrm{GaN}} N_c^{\mathrm{AlGaN}}}\exp\left(\frac{\chi^{\mathrm{GaN}} - \chi^{\mathrm{AlGaN}} - \varphi - \varphi_p}{V_T}\right), \quad (13)$$

where n_i is the carrier intrinsic concentration, N_c is the effective density of states for electrons and χ is the electron affinity.

The corresponding expressions for GaN are given as follows:

$$n = n_i^{\mathrm{GaN}}\exp\left(\frac{\varphi + \varphi_n}{V_T}\right), \quad (14)$$

$$p = n_i^{\mathrm{GaN}}\exp\left(\frac{-\varphi - \varphi_p}{V_T}\right). \quad (15)$$

The carrier intrinsic concentration is defined by

$$n_i = \sqrt{N_c N_v} \exp\left(-\frac{E_g}{2V_T}\right), \quad (16)$$

where N_v is the effective density of states for holes and E_g is the band gap.

For calculating the electron mobility in the channel of the GaN HEMT, we employ a user-specified model, which describes the mobility of a two-dimensional electron gas formed at the AlGaN/GaN heterostructure as a function of the carrier concentration and the temperature [7].

Polarization modeling is critical for GaN devices. When polarization effects are simulated, the space charge density in the Poisson equation, which is solved at the nodes located at a heterointerface, is augmented by a polarization-induced charge.

The total spontaneous polarization is defined by the difference between the values for two adjacent materials:

$$P_{sp} = P_{sp}^{\mathrm{GaN}} - P_{sp}^{\mathrm{AlGaN}}. \quad (17)$$

The relatively thick GaN layer is assumed unstrained, and so the piezoelectric component of polarization is calculated only for the thin AlGaN layer:

$$P_{pe} = 2\frac{a^{GaN} - a^{AlGaN}}{a^{AlGaN}}\left(e_{31} - \frac{e_{33}c_{13}}{c_{33}}\right), \quad (18)$$

where a is the lattice constant, e_{31} and e_{33} are the piezoelectric constants for AlGaN and c_{13} and c_{33} are the elastic constants for AlGaN.

Finally, the total polarization is determined as follows:

$$P = P_{sp} - P_{pe}. \quad (19)$$

Table I compiles the parameters for the AlN/GaN material system [8] used for the polarization simulation.

The temperature dependence of the band gaps for AlN and GaN is commonly fitted to the empirical Varshni form

$$E_g(T) = E_g(0\mathrm{K}) - \frac{\alpha T^2}{T + \beta}, \quad (20)$$

where α and β are adjustable parameters.

For AlGaN, the dependence of the band gap on composition is assumed to fit a simple quadratic form

$$E_g^{\mathrm{AlGaN}} = E_g^{\mathrm{AlN}} x + E_g^{\mathrm{GaN}}(1-x) - \gamma x(1-x), \quad (21)$$

where x is the composition and γ is the so-called bowing parameter equal to 1 [8].

The behavior of a heterojunction depends crucially on the alignment of the energy bands at the interface. According to Anderson's rule, the conduction band discontinuity (offset) is defined by the difference between the two materials electron affinities [9]:

$$\chi^{\mathrm{GaN}} - \chi^{\mathrm{AlGaN}} = \rho\left(E_g^{\mathrm{AlGaN}} - E_g^{\mathrm{GaN}}\right), \quad (22)$$

where ρ determines the portion of the band gap difference assigned to the conduction band offset. We take ρ equal to 0.7 and independent of the temperature.

The effective mass in wurtzite crystals is anisotropic. For a single band minimum described by a longitudinal mass and two transverse masses, the effective mass for the density of states is calculated as the geometric mean of the three masses:

TABLE I. PARAMETERS FOR THE POLARIZATION SIMULATION

Parameter (300 K)	Material		Units
	AlN	*GaN*	
a	3.112	3.189	Å
c_{13}	108	106	GPa
c_{33}	373	398	GPa
e_{31}	–0.5	–0.35	C/m^2
e_{33}	1.79	1.27	C/m^2
P_{sp}	-0.081	-0.029	C/m^2

$$m = \left(m_l m_t^2\right)^{1/3}, \quad (23)$$

where m_l and m_t are the longitudinal and transverse effective masses for the density of states.

Equation (23) is valid for both electrons and holes.

The effective density of states for electrons is defined through the electron effective mass as follows:

$$N_c = 2\left(\frac{2\pi m \kappa T}{h^2}\right)^{3/2}, \quad (24)$$

where h is the Planck constant.

The effective density of states for holes is defined by analogy.

Table II shows the band parameters used throughout the simulations.

With the exception of (21), the parameter values for AlGaN are linearly interpolated against composition.

B. Lattice Heat Flow Equation

Simulation of the self-heating effect implies the addition of a lattice heat flow equation to the set of the primary semiconductor device equations. According to Wachutka's thermodynamically rigorous model of lattice heating [14], in a steady-state, the lattice heat flow equation is given by

$$H = -\lambda \nabla^2 T, \quad (25)$$

where H is the heat generation rate and λ is the thermal conductivity.

The heat generation rate in the simplest form can be regarded as Joule heat:

$$H = \left(J_n + J_p\right)E. \quad (26)$$

Since the thermal conductivity is generally temperature-dependent, the following models are employed for AlN/GaN [15] and Al_2O_3 [16], respectively:

$$\lambda(T) = \lambda(300\text{K})\left(\frac{T}{300}\right)^{\delta_1}, \quad (27)$$

TABLE II. BAND PARAMETERS

Parameter	Material		Units	References
	AlN	*GaN*		
E_g (0K)	6.23	3.507	eV	[8]
α	0.001719	0.000909	eV/K	[8]
β	1462	830	K	[8]
m_l (for electrons)	$0.2938m_e$[a]	$0.1846m_e$	kg	[10]
m_t (for electrons)	$0.3433m_e$	$0.2283m_e$	kg	[10]
m_l (for holes)	$3.53m_e$	$2m_e$	kg	[11]
m_t (for holes)	$11.14m_e$	$2.04m_e$	kg	[11]
ε	8.5	9.5	–	[12][13]

a. m_e denotes the electron rest mass

$$\lambda(T) = 0.01\left(\frac{\delta_2}{T^{\delta_3}} + \delta_4 T\right), \quad (28)$$

where δ_1, δ_2, δ_3 and δ_4 are the temperature dependence coefficients.

The thermal conductivity for Si_3N_4 is taken constant and equal to 0.027 W/(cm·K) [17].

Table III shows the thermal conductivity model parameters used throughout the simulations:

TABLE III. THERMAL CONDUCTIVITY MODEL PARAMETERS

Parameter	Material		
	AlN	*GaN*	*Al_2O_3*
λ (300K)	2.85	1.3	–
δ_1	–1.64	–0.28	–
δ_2	–	–	51292
δ_3	–	–	1.2868
δ_4	–	–	0.0001769

The parameter values for AlGaN are linearly interpolated against composition.

To solve the heat flow equation, at least one thermal boundary condition must be imposed. In case of a field-effect transistor, the thermal boundary condition is commonly specified at the bottom surface of the substrate as a perfect heat sink to the room temperature and has the following form:

$$-\lambda\nabla T = \sigma(T - T_0), \quad (29)$$

where σ is the heat-transfer coefficient between a material and ambient medium, T_0 is the room temperature.

C. Trapped Charge in the Poisson Equation

Trap centers with an associated energy lying in a band gap exchange charges with the conduction and valence bands through the emission and the capture of carriers. Trap centers influence the charge distribution in semiconductor bulk. In case of acceptor traps, the space charge density in the Poisson equation is reduced by the density of states for ionized acceptor traps, which is determined as follows:

$$N_{ta}^{-} = PN_{ta}, \quad (30)$$

where N_{ta} is the density of states for acceptor traps and P is the ionization probability defined by

$$P = \frac{n}{n + \tau N_c \exp\left(\frac{E_{ta} - E_c}{V_T}\right)}, \quad (31)$$

where τ is the degeneracy factor, E_{ta} is the trap energy level and E_c is the conduction band edge.

IV. RESULTS

To investigate the effect of the presence of Fe-induced deep-level acceptor centers treated as trap states on the dc characteristics of the GaN HEMT at elevated temperatures, intentional doping of Fe is implemented for the GaN buffer layer with three different residual channel concentrations, denoted as low- (10^{16} cm^{-3}), medium- (10^{17} cm^{-3}) and high-Fe (10^{18} cm^{-3}). Fig. 2 illustrates the distributions of the Fe-induced acceptor traps with the associated energy of 0.7 eV [18] from the channel to the substrate described by a Gaussian profile with a peak concentration of $5\cdot10^{18}$ cm^{-3} at the bottom of the buffer layer to mimic the fact that the material quality deteriorates toward the substrate.

In Fig. 3, the distributions of the ionization probability for the acceptor traps are presented. As can be seen, when the acceptor trap concentration at the device channel is increased from the value of 10^{16} cm^{-3} to 10^{18} cm^{-3}, the thickness of the buffer layer where the traps are almost completely ionized ($P \geq 0.99$) decreases from the value of 0.088 μm to 0.030 μm. For low-Fe, the trap centers are not ionized ($P \leq 0.01$) at the distances of 0.292 μm and higher, while for high-Fe the limit is located at 0.068 μm.

The drain current vs gate voltage characteristics of the GaN HEMT at the drain voltage of 1 V are shown in Fig. 4. When the acceptor trap concentration at the channel is raised, the input characteristics are shifted in the positive direction. For low-Fe,

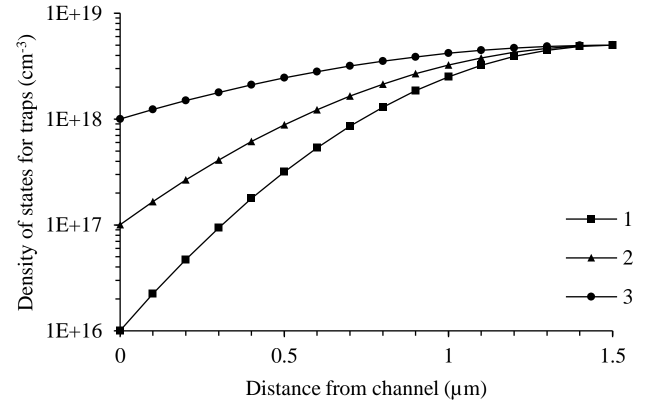

Fig. 2. Fe-induced acceptor traps distributions in the GaN buffer layer: 1 – low-Fe, 2 – medium-Fe, 3 – high-Fe

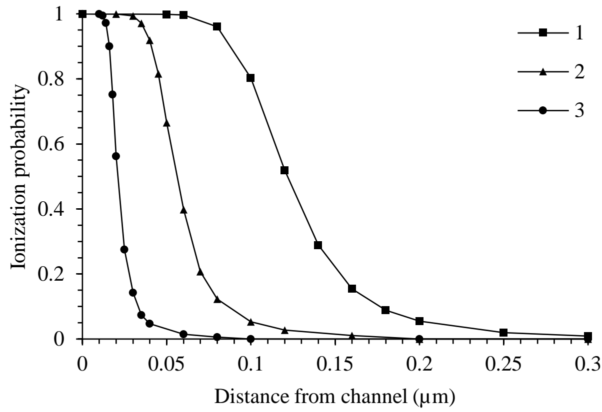

Fig. 3. Ionization probability distributions for the Fe-induced acceptor traps in the GaN buffer layer: 1 – low-Fe, 2 – medium-Fe, 3 – high-Fe

the threshold voltage equals to –3.4 V, while for high-Fe, the threshold voltage is –2.4 V.

The drain current vs drain voltage characteristics of the GaN HEMT at the gate voltage of 0 V are presented in Fig. 5. The shift of the input curves caused by the acceptor traps leads to a decrease in the drain current at the same bias conditions. For instance, at the gate voltage of 0 V and the drain voltage of 6 V, the drain current is 0.255 A for low-Fe and 0.196 A for high-Fe. In all cases, the drain current decreases, when the drain voltage is raised, as a result of the self-heating effect.

CONCLUSIONS

The effect of the presence of Fe-induced deep-level acceptor centers treated as trap states on the dc characteristics of the GaN HEMT at elevated temperatures was studied. The simulation results show that the acceptor centers intentionally introduced in the buffer layer of the device cause a shift of the input characteristics in the positive direction. The distribution of the traps in the buffer layer can be subject to optimization.

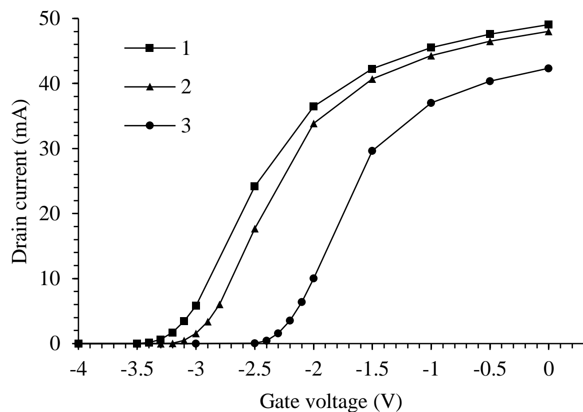

Fig. 4. Drain current vs gate voltage characteristics at the drain voltage of 1 V of the GaN HEMT: 1 – low-Fe, 2 – medium-Fe, 3 – high-Fe

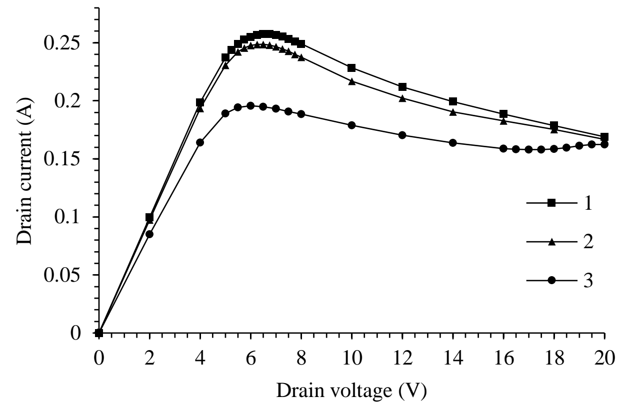

Fig. 5. Drain current vs drain voltage characteristics at the gate voltage of 0 V of the GaN HEMT: 1 – low-Fe, 2 – medium-Fe, 3 – high-Fe

ACKNOWLEDGMENT

This work was supported by the grants 3.2.04 of Belarusian National Scientific Research Program “Photonics, Opto- and Microelectronics” and T18M-108 of the Belarusian Republican Foundation for Fundamental Research.

REFERENCES

[1] K. Bejtka, R. W. Martin, I. M. Watson, S. Ndiaye, and M. Leroux, “Growth and optical and structural characterization of GaN on freestanding GaN substrates wih an (Al,In)N insertion layer,” Appl. Phys. Lett., vol. 89, pp. 191912-1–191912-3, November 2006.

[2] M. Asif Khan et al., “GaN-AlGaN heterostructure field-effect transistors over bulk GaN substrates,” Appl. Phys. Lett., vol. 76, pp. 3807–3809, April 2000.

[3] K. K. Chu et al., “9.4-W/mm power density AlGaN-GaN HEMT on free-standing GaN substrates,” IEEE Electr. Device L., vol. 25, pp. 596–598, September 2004.

[4] S. Keller et al., “Gallium nitride based high power heterojunction field effect transistors: process development and present status at UCSB,” IEEE Trans. Electron Devices, vol. 48, pp. 552–559, March 2001.

[5] W. Seifert, R. Franzheld, E. Butter, H. Sobotta, and V. Riede, “On the origin of free carriers in high-conducting n-GaN,” Cryst. Res. Tech., vol. 18, pp. 383–390, January 1983.

[6] Y. C. Choi et al., “The effect of an Fe-doped GaN buffer on off-state breakdown characteristics in AlGaN/GaN HEMTs on Si substrate,” IEEE Trans. Electron Devices, vol. 53, pp. 2926–2931, December 2006.

[7] V. Volcheck, V. Stempitsky, “Mobility of a two-dimensional electron gas in the AlGaN/GaN heterostructure: simulation and analysis,” unpublished.

[8] I. Vurgaftman, J. R. Meyer, and L. R. Ram-Mohan, “Band parameters for III-V compound semiconductors and their alloys,” J. Appl. Phys., vol. 89, pp. 5815–5875, June 2001.

[9] R. L. Anderson, “Germanium-gallium arsenide heterojunctions,” IBM J. Res. Dev., vol. 4, pp. 283–287, July 1960.

[10] M. Goano, E. Belotti, E. Ghillino, G. Ghione, and K. F. Brennan, “Band structure onlocal pseudopotential calculation of the III-nitride wurtzite phase materials system. Part I. Binary compounds GaN, AlN, and InN,” J. Appl. Phys., vol. 88, pp. 6467–6475, December 2000.

[11] K. Kim, W. R. L. Lambrecht, B. Segall, and M. van Schilfgaarde, “Effectve masses and valence-band splittings in GaN and AlN,” Phys. Rev. B, vol. 56, pp. 7363–7375, September 1997.

[12] I. Akasaki and M. Hashimoto, “Infrared latice vibration of vapour-grown AlN,” Solid State Commun., vol. 5, pp. 851–853, 1967.

[13] A. S. Barker Jr. and M. Ilegems, “Infrared lattice vibrations and free-electron dispersion in GaN,” Phys. Rev. B, vol. 7, pp. 743–750, January 1973.

[14] G. H. Wachutka, “Rigorous thermodynamic treatment of heat generation and conduction in semiconductor device modeling,” IEEE Trans. Comput.-Aided Des., vol. 9, pp. 1141–1149, November 1990.

[15] J. Piprek, Semiconductor Optoelectronic devices” Introduction to Physics and Simulation. San Diego, CA: Academic Press, 2003.

[16] A. M. Hofmeister, “Thermal diffusivity and thermal conductivity of single-crystal MgO and Al_2O_3 and related compounds as a function of temperature,” Phys. Chem. Minerals, vol. 41, pp. 361–371, January 2014.

[17] M. T. Alam, M. P. Manoharan, M. A. Haque, C. Muratore, and A. Voevodin, “Influence of strain on thermal conductivity of silicon nitride thin films,” J. Micromech. Microeng., vol. 22, pp. 1–8, March 2012.

[18] M. Silvestri, M. J. Uren, and M. Kuball, “Iron-induced deep-level acceptor center in GaN/AlGaN high electron mobility transistors: energy level and cross section,” Appl. Phys. Lett., vol. 102, pp. 073501-1–073501-4, February 2013.